Optical resolution of baclofen *via* diastereomeric salt pair formation between 3-(*p*-chlorophenyl)glutaramic acid and (*S*)-(−)-α-phenylethylamine

Mino R. Caira,*[a] Rainer Clauss,[b] Luigi R. Nassimbeni,[a] Janet L. Scott[b] and Alexander F. Wildervanck[a]

[a] *Department of Chemistry, University of Cape Town, Rondebosch 7700, South Africa*
[b] *Fine Chemicals Corporation, Eppindust, South Africa*

The structures of the diastereomeric salts of (*R*)-(+)- and (*S*)-(−)-3-(*p*-chlorophenyl)glutaramic acid with (*S*)-(−)-phenylethylamine have been determined by X-ray crystallography. Solubility and melting behaviours of the salts were analysed and correlated with their structural properties in the solid state. The (*R*)-(+)-3-(*p*-chlorophenyl)glutaramic acid was converted to (*R*)-(−)-baclofen *via* a Hofmann degradation (57% yield, 99.8% ee, enantiomeric excess).

Introduction

3-(*p*-Chlorophenyl)glutaramic acid (GAM) is an intermediate in the synthesis of baclofen [4-amino-3-(4-chlorophenyl)butyric acid][1] (Scheme 1). (±)-Baclofen is the most lipophilic analogue

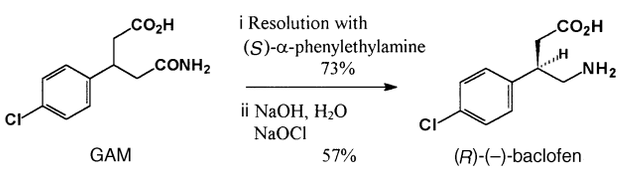

Scheme 1

of GABA (γ-aminobutyric acid) and is used clinically for the treatment of spasticity of spinal and cerebral origin.[2] Literature observations suggest that the biological activity of baclofen resides in the (−)-enantiomer.[3] The *R* configuration has been assigned to this enantiomer on the basis of X-ray crystallography.[4] Previously, pure enantiomers of the drug have been analysed or prepared by various HPLC separation methods,[5] stereospecific syntheses[6] or chemoenzymatic syntheses.[7] Optical resolution by fractional crystallisation of diastereomeric salts is still widely employed in industry as a useful procedure for the commercial preparation of optically active compounds.[8] Only β-phenyl-GABA has been resolved by fractional crystallisation of the cinchonidine[9] or α-phenylethylamine[10] salts. Resolution of 4-phenylglutaramic acid has been effected through the salt with D(−)-threo-2-amino-1-(*p*-nitrophenyl)-propane-1,3-diol,[11] and is to date the only report of a chiral glutaramic acid resolved by the classical resolution method.

Amongst the numerous reports accounting for diastereomeric salt mediated resolutions, relatively few have probed the crystal structures of these salt pairs in attempts to gain insight into recognition mechanisms. Various studies have investigated structural evidence for the differing physicochemical properties that allow for efficient diastereomeric salt separations from solution.[12] It often appears that differing physicochemical properties of diastereomeric salts cannot be explained on the basis of differences in strong interactions only, but that weak second-order van der Waals interactions and subtle electrostatic effects may also play a key role.

We have resolved (±)-GAM by diastereomeric salt formation with (*S*)-(−)-α-phenylethylamine (*S*PEA) into its two enantiomers (*R*)-(+)-GAM (*R*GAM) and (*S*)-(−)-GAM (*S*GAM). The *R*GAM was subsequently converted to (*R*)-(−)-baclofen *via* a Hofmann degradation. The crystal structures of both diastereomeric salts, (*S*PEA)(*R*GAM) **1** and (*S*PEA)(*S*GAM) **2**, were analysed to gain possible structural evidence of the differential solubilities of the two salts.

Experimental

Thermal analysis

Melting points were determined by means of differential scanning calorimetry (DSC). A Perkin-Elmer PC7 Series thermal analysis system was employed. Samples (of masses ranging from 3–8 mg) were ground to a fine powder, placed in vented aluminium pans and heated at a constant rate of 10 °C min^{-1}. The sample chamber was purged with N_2 gas at a flow rate of 30 ml min^{-1}.

Polarimetry

Optical rotations were measured on a Perkin-Elmer 141 Polarimeter to an accuracy of ±0.005°. Rotation measurements of (*R*)-(−)-baclofen were not possible due to the insolubility of the drug in most organic solvents. A sample of our enantiopure baclofen was submitted to Fine Chemicals Corporation for chiral HPLC analysis on a (D)-penicillamine column (2 mM aq. $CuSO_4$ mobile phase).

Solubility determination

For **1** and **2** this was performed in MeOH by UV spectrophotometry, using a Philips PU8700 series UV–VIS spectrophotometer. Standard solutions (at 24 °C) were made in the concentration range 0.25–1.5 mg ml^{-1}. The linear relationship $A = 1.050\ C$ (A = absorbance and C = concentration in mg ml^{-1}) was established by measuring absorbances at $\lambda_{max} = 260.6$ nm (correlation coefficient $r = 0.9998$).

X-Ray powder patterns

These were measured on a Philips PW 1050/80 goniometer with Ni-filtered Cu-Kα radiation ($\lambda = 1.5418$ Å). Step scans of 0.1° 2θ over the range $6° \leqslant 2\theta \leqslant 40°$, 2 s per step, were performed using automatic divergence and receiving slits. The program LAZY PULVERIX[13] was used to generate idealised XRD patterns for both co-crystals from the determined single crystal X-ray structures. Input data comprised space group information, unit cell parameters, atomic coordinates and thermal parameters.

Table 1 Crystal data and structure refinement for **1** and **2**

	1	**2**
Empirical formula	$C_{19}H_{23}ClN_2O_3$	$C_{19}H_{23}ClN_2O_3$
Formula mass/g mol^{-1}	362.84	362.84
Space group	$P2_1$	$P2_1$
a/Å	5.728(2)	14.344(3)
b/Å	20.671(3)	5.474(1)
c/Å	8.354(1)	14.434(2)
β/°	107.39(2)	114.75(2)
V/Å^3	943.9(4)	1029.4(3)
Z	2	2
D_c/g cm^{-3}	1.277	1.171
D_m/g cm^{-3}	1.269	—
Absorption coefficient/mm^{-1}	0.222	0.204
F(000)	384	384
Data collection (24 °C)		
Crystal size/mm	0.4 × 0.5 × 0.3	0.3 × 0.3 × 0.3
Range scanned, θ/(°)	1.97–24.97	1.55–24.99
Index ranges	h: ±6; k: −24; 0; l: 0, 9	h: ±15; k: 0, 6; l: 0, 17
Reflections collected	1837	2110
Independent reflections	1703 [R(int) = 0.0301]	2026 [R(int) = 0.0383]
Data/restraints/parameters	1703/6/253	2026/0/138
Final R indices [$I > 2\sigma(I)$]	$R1$ = 0.0296, $wR2$ = 0.0938	$R1$ = 0.1258, $wR2$ = 0.3111
R indices (all data)	$R1$ = 0.0387, $wR2$ = 0.1075	$R1$ = 0.2244, $wR2$ = 0.3134
Flack parameter x	−0.12(9)	0.0(5)
Largest diff. peak and hole/e Å^{-3}	0.202 and −0.236	0.499 and −0.345

Single crystal X-ray analyses

Single crystals of **1** and **2** were grown from MeOH and MeOH–acetone (9:1), respectively. Intensity data were measured on an Enraf-Nonius CAD4 diffractometer at 294 K using graphite-monochromated Mo-Kα radiation (λ = 0.710 69 Å). Accurate cell dimensions were obtained by least-squares refinement of 24 accurately measured reflections. Data in the range $1° \leqslant \theta \leqslant 25°$ were collected in the ω–2θ scan mode with a maximum recording time of 40 s per reflection. Intensity control was performed every hour by means of three reference reflections and orientation control every 200 reflections. Measured intensities were corrected by Lorentz–polarisation factors as well as an empirical absorption correction.[14]

The structures were solved by direct methods using the program SHELX-86[15] and refined on F^2 by full-matrix least-squares techniques using SHELX-93.[16] Polar axis restraints after Flack and Schwarzenbach[17] were used to define the origin of the polar space group $P2_1$. For **1** all non-hydrogen atoms were located in difference electron density syntheses and refined anisotropically. All hydrogen atoms, except those of the $-NH_3^+$ group, were located and placed in geometrically generated positions and refined with positional parameters riding on the parent atom (C–H = 1.00 Å). The $-NH_3^+$ H atoms were refined with bond length restraints only. Chemically equivalent hydrogen atoms were tied to common isotropic thermal parameters which were allowed to refine. No hydrogen atoms could be located in **2** and these were therefore omitted from the model. All phenyl rings were refined as idealised hexagons with common variable isotropic thermal parameters. Refinement with the carbon atoms of ring A included gave rise to peaks in the electron density surrounding the phenyl ring suggesting an alternative orientation (ring B) inclined at 72° to the plane of ring A (Fig. 4). This was modelled by allowing two possible orientations of the phenyl ring whose site occupancy factors were refined to 0.52 and 0.48 for rings A and B, respectively. Details of the crystal data and refinement parameters appear in Table 1.

Atomic coordinates, bond lengths and angles, and thermal parameters have been deposited at the Cambridge Crystallographic Data Centre (CCDC). For details of the deposition scheme, see 'Instructions for Authors', *J. Chem. Soc., Perkin Trans. 2*, 1997, Issue 1. Any request to the CCDC for this material should quote the full literature citation and the reference number 188/57.

Resolution of (±)GAM

(±)GAM (18 g, 74.4 mmol) was dissolved in methanol (250 ml) and warmed to approximately 60 °C. *S*PEA (9.48 ml, 74.4 mmol) was carefully added *via* a graduated pipette, and the warm solution stirred for a few minutes. The resulting 1:1 (±)GAM–*S*PEA solution was cooled to room temperature and left to stand in the dark for approximately 24 h affording colourless plate-like crystals of **1** (9.86 g; 73%), mp 187–197 °C, $[\alpha]_D^{24}$ = +5.5 (*c* 1.0 in MeOH). The crystals were isolated by filtration, dried and dissolved in water (200 ml) by heating to approximately 90 °C. 3 M HCl (90.5 ml) was added at this temperature after which the solution was allowed to cool to room temperature. The precipitate was filtered, washed with water and vacuum-dried to give *R*GAM (6.23 g, 95%), mp 173 °C (Found: C, 54.62; H, 4.98; N, 5.72. $C_{11}H_{12}ClNO_3$ requires C, 54.67; H, 4.96; N, 5.79%); $[\alpha]_D^{24}$ = +9.5 (*c* 1.0 in MeOH). The mother liquor of the crystallisation was isolated and concentrated by evaporation. Any further precipitate was removed from the solution by filtration (*ca.* 2 g salt). The filtrate evaporated to dryness and the contaminated (*S*PEA)(*S*GAM) **2** salt was recrystallised twice from methanol–acetone (9:1) (7.1 g, 53%), mp 185–190 °C; $[\alpha]_D^{24}$ = −12.3 (*c* 1.0 in MeOH). This salt, when acidified in water, yielded *S*GAM, $[\alpha]_D^{24}$ = −9.5 (*c* 1.0 in MeOH).

(*R*)(−)-Baclofen

The conversion of *R*GAM to (*R*)-(−)-baclofen was effected by the Hofmann reaction using the experimental details previously reported.[1] *R*GAM (6.57 g, 27.21 mmol) was added to a solution of sodium hydroxide (2.8 g, 69.4 mmol) in water (50 ml) at 24 °C. A 10.8% aqueous solution of sodium hypochlorite (28.3 g) was then added over 2.5 h at 0 °C *via* a dropping funnel. The solution was stirred for a further 12 h at room temperature (approximately 24 °C) after which time it was carefully neutralised (pH 7.5) with dilute hydrochloric acid. The precipitate was filtered off at the pump and washed with water. The precipitate was boiled in methanol to remove the last traces of *R*GAM and filtered to yield pure (*R*)-(−)-baclofen (1.30 g, 22% yield). The mother liquors were reduced in volume *in vacuo* to yield more product which was boiled in methanol and filtered to give another 2.05 g of (*R*)-(−)-baclofen (3.35 g total, 57%), mp 205–208 °C (Found: C, 56.30; H, 5.78; N, 6.52. $C_{10}H_{12}ClNO_2$ requires C, 56.21; H, 5.66; N, 6.56%). The HPLC procedure described above had a 0.2% detection limit for (*S*)-(+)-

Table 2 Selected torsion angles

	1	2
C(6)–C(3)–C(4)–C(5)	174.1(3)	−179(2)
C(6)–C(3)–C(2)–C(1)	−49.6(3)	62(2)
C(2)–C(3)–C(6)–C(11)	114.5(3)	−137(1)
O(13)–C(1)–C(2)–C(3)	−65.8(3)	−153(1)
O(15)–C(5)–C(4)–C(3)	−29.8(4)	40(4)
N(25)–C(18)–C(19)a–C(20)a	−42.2(4)	−20(4)
N(25)–C(18)–C(19)b–C(20)b		−83(3)

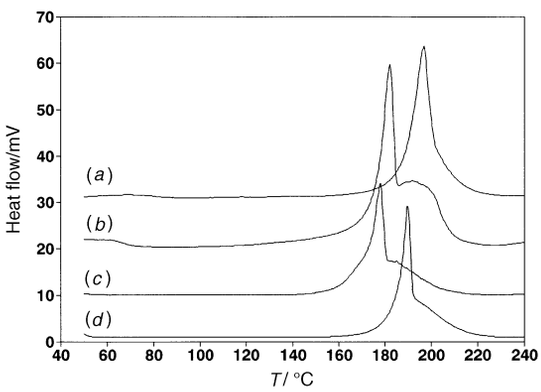

Fig. 1 Melting curves of various fractions of the resolution: (*a*) pure **1**, (*b*) **1** and **2** in a 1:1 mixture, (*c*) **1** and **2** in a 18:82 mixture, (*d*) pure **2**

baclofen. The chromatogram of the final product showed no trace of the (*S*)-enantiomer, thus indicating a minimum ee of 99.8% for (*R*)-(−)-baclofen.

Results and discussion

Thermal analysis

Fig. 1 shows DSC traces of the two diastereomeric salts **1** [trace (*a*)] and **2** [trace (*d*)]. Trace (*b*) corresponds to a 1:1 mixture of the diastereomers and trace (*c*) to a **1** = 0.18–**2** = 0.82 mixture of the diastereomers. The sample giving trace (*c*) was isolated from a MeOH solution saturated with **1** and **2** (*i.e.* having the eutectic composition as calculated from the ternary phase diagram). Hot stage microscopy gave evidence that the endotherms following the eutectic melt in (*c*) and the melt in (*d*) could be due to decomposition rather than fusion of the diastereomer in excess. It appears that the melting points of pure **1** and **2** [using the peak values in traces (*a*) and (*d*)] differ by approximately 7 °C.

Solubility diagram

The possibility of scaling up this separation process for industrial purposes prompted the need to optimise the crystallisation conditions such that yield and purity were maximal. Single crystal structure analysis and XRD powder patterns of various fractions of the resolution process proved the absence of racemic crystals, solvates or solid solutions. The solubilities of **1** and **2** were 32 ± 1 and 136 ± 5 mg ml^{-1}, respectively. Fig. 2 indicates the eutectic composition (18% **1** and 82% **2**) as established by polarimetry and UV spectrophotometry. Three intermediate points on the (*S*PEA)(*R*GAM) branch of the isotherm (24 °C) were established by dissolving accurately weighed amounts of both salts in 5 ml MeOH and assuming complete dissolution of the more soluble (*S*PEA)(*S*GAM) salt. The efficiency $S = (1 - 2X_{eu})/(1 - X_{eu})$ of the resolution [18] as calculated from the eutectic was 0.78 and the observed efficiency [19] $S = OP \times Y$ (OP = optical purity, Y = yield of precipitated salt) was 0.73.

Crystal structure analyses

The atom numbering Schemes of **1** and **2** are given in Figs. 3(*a*) and 3(*b*) respectively. Relative to *S*PEA the absolute configuration of GAM in **1** was assigned as the (*R*) configuration. The high thermal motions of both the amide and carboxylate moieties in **2** complicated configuration determination because the latter depends on distinguishing between an oxygen and a nitrogen atom. Assignment was therefore made by means of hydrogen bonding characteristics and supplementary polarimetry experiments. The conformations of the *R* and *S* enantiomers of GAM in **1** and **2** are essentially similar, differing mainly in the characteristic C(2)–C(3)–C(6)–C(11) torsion angle (see Table 2). The C(18)–C(19)b bond length (1.72 Å) and N(25)–C(18)–C(19)b bond angle (96.7°) of *S*PEA in **2** (Fig. 4) make no real chemical sense and are clearly artefacts attributable to the poor quality of the intensity data. In addition, the fact that the plane of ring B (φB) is almost parallel to the 5.72 Å *b* axis (angle between φB and the *b*-axis = 5.5°) results in abnormally short (3 Å) C ··· C contacts. Ring B is therefore omitted in subsequent packing diagrams to avoid unnecessary confusion. The characteristic torsion angle N(25)–C(18)–C(19)–C(20)a shows a disfavoured *syn*-periplanar N(25) ··· φA interaction in **2** as opposed to the synclinal N(25) ··· φ interaction in **1**. Deprotonation of *R*GAM in **1** was confirmed by the equidistant C(1)–O(13) and C(1)–O(14)

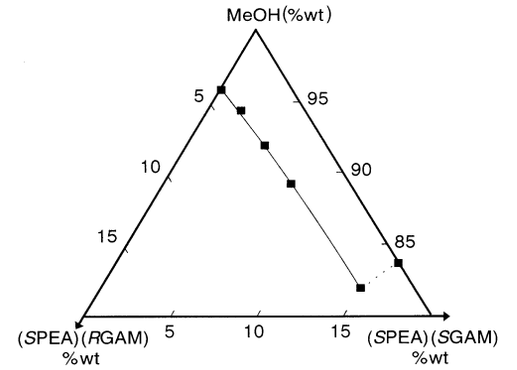

Fig. 2 Solubility diagram of **1** and **2** in MeOH

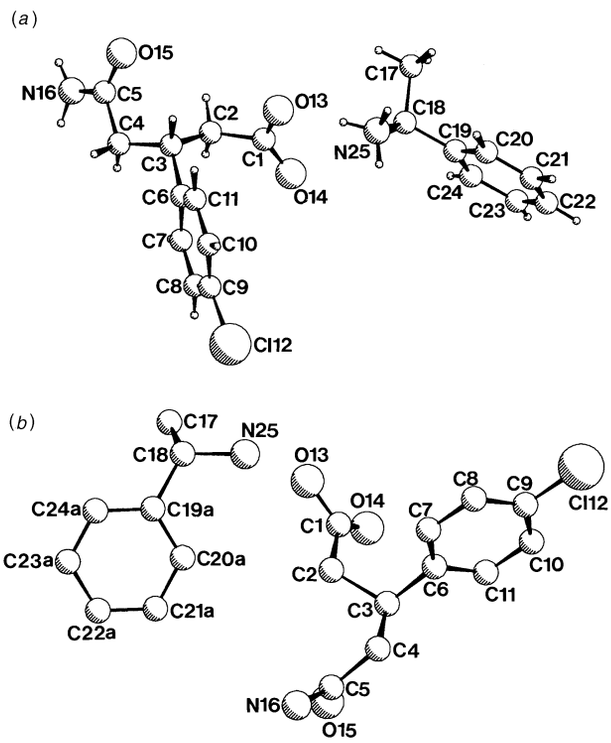

Fig. 3 (*a*) Asymmetric unit of **1** indicating atom numbering scheme. (*b*) Asymmetric unit of **2** indicating atom numbering scheme. Only φA is represented in the diagram.

Table 3 Hydrogen bond data. Some of these bonds are shown in Fig. 5(*a*) and (*b*) and are labelled **a**, **b**, **c** and **d**

	D–H···A	D–H/Å	D···A/Å	H···A/Å	D–H···A/(°)
1					
a	N(25)–H(253)···O(13)	0.94(3)	2.720(3)	1.79(3)	173(4)
b	N(25)–H(251)···O(14)^{i}	0.96(4)	2.763(3)	1.81(3)	173(3)
c	N(25)–H(252)···O(15)^{ii}	0.95(3)	2.806(4)	1.86(3)	175(3)
d	N(16)–H(161)···O(14)^{iii}	0.84(5)	2.962(4)	2.16(5)	159(4)
2					
a	N(25)···O(13)		2.71(2)		
b	N(25)···O(13)^{iv}		2.80(1)		
c	N(25)···O(14)^{v}		2.82(2)		
d	N(16)···O(15)^{vi}		2.93(2)		
	N(16)···O(15)^{v}		3.26(6)		

^{i} $x-1, y, z$. ^{ii} $x-1, y, z-1$. ^{iii} $x+1, y, z+1$. ^{iv} $1-x, y-\frac{1}{2}, 1-z$. ^{v} $x, y-1, z$. ^{vi} $-x, y-\frac{1}{2}, -z$.

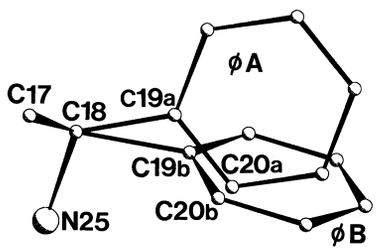

Fig. 4 The disordered phenyl ring of *S*PEA in **2**

bond lengths in the carboxylate moiety [1.248(3) and 1.257(3) Å respectively]. Three H atoms were located in tetrahedral geometry around the nitrogen atom, N(25). Proton transfer in **2** could not readily be deduced from structural evidence since the C(1)–O(13) and C(1)–O(14) bond lengths, 1.30(2) and 1.22(3) Å respectively, differed significantly. Disorder in **2** clearly places a limit on the accuracy of its molecular parameters.

Two distinct hydrogen bonding networks are found in **1** and **2**. Table 3 lists the hydrogen bonds found in the two crystal structures and Fig. 5 shows packing diagrams illustrating these (see Fig. 6 for stereodiagrams). In both structures the N atom of *S*PEA forms three hydrogen bonds to various oxygen atoms of GAM. In **1**, the amide and carboxylate moieties are hydrogen bonded to an ammonium cation, the latter in turn interlinking the rings so formed by a fourth N–H···O hydrogen bond. This 'chain of rings' network runs perpendicular to the polar axis resulting in alternating hydrophobic and hydrophilic layers. In **2**, two carboxylate moieties are hydrogen bonded to the N atom of *S*PEA. The amide moieties are separately hydrogen bonded to one another. Both these separate amide···amide and carboxylate···carboxylate interaction networks form helical chains running parallel to the polar axis. This gives rise to alternating hydrophobic and hydrophilic columns interspersed throughout the crystal (interestingly the plate-like crystal morphology of **1** also contrasted with the long rod-like 'fibre' crystals of **2**). The two distinct XRD powder patterns of the pure diastereomeric salts were recorded. Both these patterns showed excellent agreement with the powder patterns computed from the single crystal structure data.

Possible structural evidence for the chiral discrimination

For a comparative study we isolated the region in the crystal bearing the nitrogen atom of the resolving agent [N(25)] and performed a detailed study on the nature of interactions of this atom with both *R*GAM and *S*GAM. Table 4 shows the geometry of the hydrogen bonded acceptor oxygen atoms around this nitrogen atom. In **2** the acceptor oxygens are slightly more

Table 4 Orientation of hydrogen bond acceptors around the N atom of *S*PEA. Superscript roman numerals refer to the symmetry operators in Table 3

1		**2**	
C–N···O(13)	109.5(2)°	C–N···O(13)	117(1)°
C–N···O(14)^{i}	111.9(1)°	C–N···O(13)^{iv}	113(1)°
C–N···O(15)^{ii}	117.1(2)°	C–N···O(14)^{v}	124(1)°
O(13)···N···O(14)^{i}	108.3(1)°	O(13)···N···O(13)^{iv}	98(1)°
O(13)···N···O(15)^{ii}	103.9(1)°	O(13)···N···O(14)^{v}	98(1)°
O(14)^{i}···N···O(15)^{ii}	105.5(1)°	O(13)^{iv}···N···O(14)^{v}	103(1)°

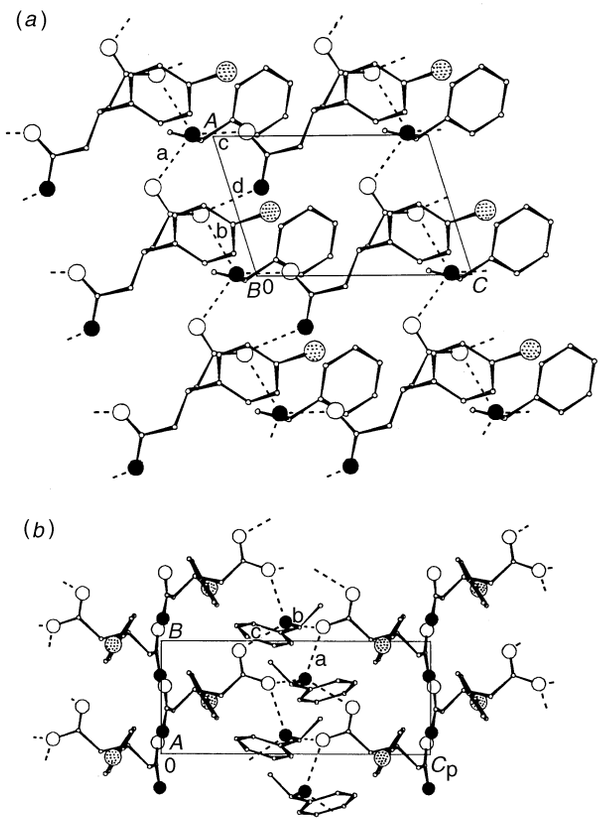

Fig. 5 (*a*) Packing diagram of the crystal structure of **1** viewed as projected down [010]. Nitrogen atoms are represented by solid, chlorine by shaded and oxygen by open circles. The labelled hydrogen bonds are referred to in Table 3. (*b*) Packing diagram of the crystal structure of **2** viewed as projected down [100]. The labelled hydrogen bonds are referred to in Table 3.

puckered around the nitrogen donor and are not as 'tetrahedrally arrayed' as in **1**.

An extensive survey of the Crystallographic Structural Database (CSD) for N–H···O=C hydrogen bonding patterns found the distribution of N–H···O angles consistent with an overall geometric preference for a linear or nearly linear N–H···O arrangement.[20] Murray-Rust and Glusker have also found that hydrogen bonds involving a keto oxygen atom as the acceptor (X–H···O=C<, X = O, N) prefer an H···O=C< angle of *ca.* 135°.[21] A quantitative measure of comparative hydrogen bond stabilities is the computation of their potential functions as demonstrated by Vedani and Dunitz.[22] The authors used a modified Lennard-Jones potential function accounting for directionality factors [eqn. (1)], where coefficients A' and C'

$$E_{\mathbf{HB}} = (A'/r'^{12}_{\mathbf{H}\cdots\mathrm{A}} - C'/r'^{10}_{\mathbf{H}\cdots\mathrm{A}}) \cos^{k}(\theta_{\mathbf{D}-\mathrm{H}\cdots\mathrm{A}}) \cos^{m} (\chi_{\mathbf{H}\cdots\mathrm{A}-\mathrm{AA}} - \chi_{\mathbf{0}}) \cos^{n}(\omega_{\mathbf{H}\cdots\mathrm{A}-\mathrm{AA}-\mathrm{AB}} - \omega_{\mathbf{0}}) \quad (1)$$

depend on various factors such as the donor and acceptor atom type. The various symbols are explained in Fig. 7. If we assume the N–H···O angles to be 180° and $r_{\mathbf{H}\cdots\mathrm{O}}$ to be con-

Table 5 Geometry of acceptor oxygens hydrogen bonded to the N atom of *S*PEA. Superscript roman numerals refer to the symmetry operators in Table 3

	1				**2**		
	N···O–C	N···O–C–O[a]	$\|E_{HB}\|$		N···O–C	N···O–C–O[a]	$\|E_{HB}\|$
O(13)	106.1°	2.2°	$0.77K_1$	O(13)	127.8°	3.8°	$0.97K_1$
O(14)[i]	122.0°	7.6°	$0.93K_1$	O(13)[iv]	118.9°	48.3°	$0.41K_1$
O(15)[ii]	127.0°	13.5°[b]	$0.93K_1$	O(14)[v]	104.7°	24.4°	$0.62K_1$

[a] *I.e.* angle between the N···O vector and the O–C–O (carboxylate) plane. [b] In this case we refer to the O–C–N (amide) plane.

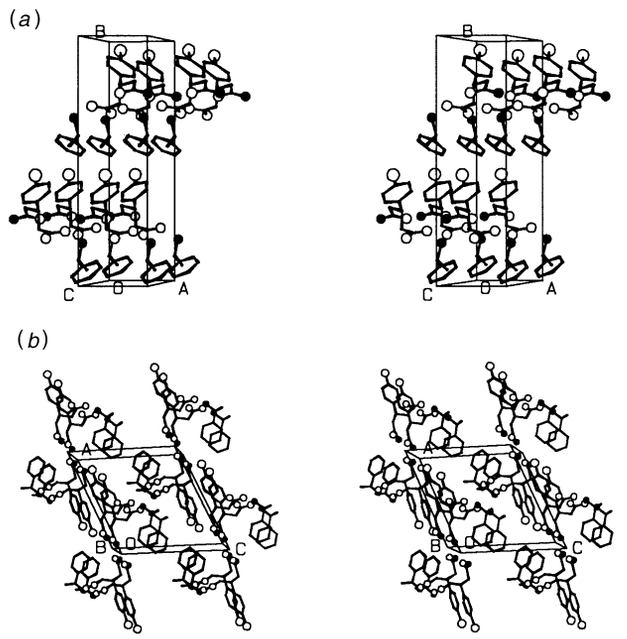

Fig. 6 (*a*) Stereodiagram of **1** showing the distinct alternating hydrophobic and hydrophilic layers perpendicular to the polar axis. Nitrogen atoms are represented by solid circles. (*b*) Stereodiagram of **2** showing an inclined view down the unique axis illustrating the helical N···O interactions.

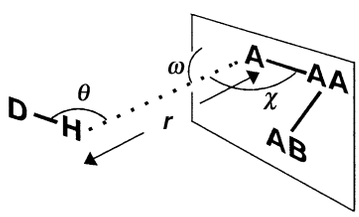

Fig. 7 Diagram illustrating the parameters in eqn. (1). D = donor, A = acceptor, AA and AB are selected atoms defining the acceptor plane.

stant for the hydrogen bonds involving the N atom of *S*PEA (so as to bypass the problem of the absence of the H coordinates in **2**) we may obtain a quantitative measure of relative interaction stabilities due to lone-pair directionality preferences at the acceptor atoms. We thus only compare the overall energetic preferences of the donor orientations around the three acceptor oxygens hydrogen bonded to N(25) [*i.e.* the last two terms of eqn. (1)]. Eqn. (1) then reduces to eqn. (2) where K_1 is a

$$|E_{HB}| = K_1 \cos^m(\chi_{N\cdots O-C} - \chi_0) \cos^n(\omega_{N\cdots O-C-O} - \omega_0) \quad (2)$$

constant, $\chi_0 = 135°$ and $\omega_0 = 0°$ for sp^2 hybridised carboxyl oxygen atoms, and $m = n = 2$ for carboxyl oxygens.[22] Table 5 compares the relative E_{HB} values calculated from the angles listed.

Calculating E_{HB} values is complicated by oxygen atoms accepting hydrogen bonds from two donors, as well as some acceptors being carboxylate anions and other amides. The relative absolute values nevertheless point towards orientational energetic preferences of isolated regions in the crystal structures which is reflected in the relative diastereomer stabilities.

Conclusions

We have found an efficient and easy route to large scale production of (*R*)-(−)-baclofen. We have isolated both diastereomeric salts and characterised these in order to optimise the process and find possible explanations for the preferential crystallisation of *S*PEA with *R*GAM. Chiral 'lock' and chiral 'key' analogies[23] are often used in justifying discrimination in host–guest chemistry. Structurally small (*i.e.* low molecular mass) drug molecules interacting with small resolving agent molecules yield highly intricate interaction networks increasing the variables controlling chiral recognition to such an extent that it becomes difficult to isolate those variables that play the primary role in stereospecificity. We summarise some of the stereochemical and physicochemical differences between **1** and **2** that provide a reasonable basis for explaining the separation efficiency:

(*a*) Separate carboxylate···ammonium···carboxylate and amide···amide interactions in **2** *vs.* carboxylate···ammonium···amide interactions in **1**.

(*b*) Quantitative comparison of hydrogen bond potential energies for those bonds involving the nitrogen atom of *S*PEA (regarded as the primary interaction site) illustrated the overall directional energetic preference of the hydrogen bonds in **1**.

(*c*) Calculated crystal densities differed by 8.3%, the higher density of **1** being indicative of a more efficient diastereomeric assembly.

(*d*) The solubilities of **1** and **2** differed by a factor of 4.

No convincing differences in second order C···O, C···N or phenyl ring interactions were found. Interpreting this in terms of the 'three-point' contact model of chiral recognition,[24] the structural evidence for the ion-pairing behaviour was found mainly in the stability of the primary dimeric contacts rather than the secondary dimer–dimer oligomeric contacts.

References

1 K. Rudnick and K. Bochow, *Ger. Pat.* DD 234 162, 1986; *Chem. Abstr.* 1987, **106**, 4530c.
2 P. Hudgson and D. Weightman, *Brit. Med. J.*, 1971, **4**, 15.
3 H. R. Olpe, H. Demiéville, V. Baltzer, W. L. Benzce, W. P. Koella, P. Wolf and H. L. Haas, *Eur. J. Pharmacol.*, 1978, **52**, 133.
4 C. H. Chang, D. S. C. Yang, C. Y. Chung, W. Bi-Cheng, J. Pletcher, M. Sax and C. F. Terrence, *Acta Crystallogr., Sect. B*, 1982, **38**, 2065.
5 (*a*) E. W. Wuis, E. W. J. Beneken Kolmer, L. E. C. van Beijsterveld, R. C. M. Burgers, T. B. Vree and E. v d Kleyn, *J. Chromatogr.*, 1987, **451**, 419; (*b*) C. Vaccher, P. Berthelot and M. Debaert, *J. Chromatogr.*, 1993, **45**, 95; (*c*) A. Sano, S. Takitani and H. Nakamura, *Kuromatografi*, 1994, **15** (4), 234.
6 (*a*) C. Herdies and H. P. Hubmann, *Tetrahedron Asymmetry*, 1992, **3** (9), 1213; (*b*) A. Shoenfelder, A. Mann and S. Le Coz, *Synlett*, 1993, **1**, 63; (*c*) S. Yoshifuji and M. Kaname, *Chem. Pharm. Bull.*, 1995, **43**, 1302.
7 R. Chênevert and M. Desjardins, *Can. J. Chem.*, 1994, **72**, 2312.
8 *Chirality in Industry*. A. N. Collins, G. N. Sheldrake and J. Crosby, ed., Wiley, London, 1992, p. 20.

9 M. Sobocinska, G. Kupryszewski and M. M. Zobaczewa, *Rocz. Chem.*, 1974, **48**, 461.
10 N. A. Sivov, R. A. Gracheva, V. M. Potapov, L. G. Polevoi and I. P. Neumyvakin, *Otkrytiya, Izobret., Prom. Obraztsy, Tovarnye Znaki*, 1981, **17**, 88 [*Pat. USSR* 827480/7 May (1981)].
11 F. Morlacchi, V. Losacco and V. Tortorella, *Gazz. Chim. Ital.*, 1975, **105**, 349.
12 See for example: (*a*) R. Yoshioka, O. Ohtsuki, T. Da-Ta, K. Okamura and M. Senuma, *Bull. Chem. Soc. Jpn.*, 1994, **67**, 3012; (*b*) F. J. J. Leusen, H. J. Bruins Slot, J. H. Noordijk, A. D. van der Haest, H. Wynberg and A. Bruggink, *Recl. Trav. Chim. Pays-Bas*, 1992, **111**, 111; (*c*) M. Czugler, I. Csöregh, A. Kálmán, F. Faigl and M. Ács, *J. Mol. Struct.*, 1989, **196**, 157.
13 K. Yvon, W. Jeitschko and E. J. Parthé, *J. Appl. Crystallogr.*, 1977, **10**, 73.
14 A. C. T. North, D. C. Philips and F. S. Matthews, *Acta Crystallogr., Sect. A*, 1968, **24**, 351.
15 G. M. Sheldrick, SHELX-86, in *Crystallographic computing 3*, eds. G. M. Sheldrick, C. Kruger and R. Goddard, Oxford University Press, Oxford, 1985, p. 175.
16 G. M. Sheldrick, SHELX-93: A program for Crystal Structure Determination, *J. Appl. Crystallogr.*, in preparation, 1993.
17 H. D. Flack and D. Swarzenbach, *Acta Crystallogr., Sect. A*, 1988, **44**, 499.
18 D. Kozma, G. Pokol and M. Ács, *J. Chem. Soc., Perkin Trans. 2*, 1992, 435.
19 E. Fogassy, A. Lopata, F. Faigl, F. Darvas and M. Ács, *Tetrahedron Lett.*, 1980, **21**, 647.
20 R. Taylor, O. Kennard and W. Versichel, *Acta Crystallogr., Sect. B*, 1984, **40**, 280.
21 P. Murray-Rust and T. Glusker, *J. Am. Chem. Soc.*, 1984, **106**, 1018.
22 A. Vedani and J. D. Dunitz, *J. Am. Chem. Soc.*, 1985, **107**, 7653.
23 F. Toda, *Supramolecular Chemistry*, 1995, **6**, 159.
24 M. Ács, *Acta Chim. Hung.—Models in Chemistry*, 1995, **132**, 409.

Paper 6/06037D
Received 2*nd September* 1996
Accepted 25*th November* 1996